Enhanced Primary Frequency Control from EVs: a Fleet Management Strategy to Handle Discrete Responses

Zecchino, Antonio; D'Arco, Salvatore ; Endegnanew, Atsede G. ; Korpås, Magnus; Marinelli, Mattia

Published in:
IET Smart Grid

Link to article, DOI:
10.1049/iet-stg.2018.0274

Publication date:
2019

Document Version
Peer reviewed version

Enhanced Primary Frequency Control from EVs: a Fleet Management Strategy to Mitigate Effects of Response Discreteness

Antonio Zecchino [1], Salvatore D'Arco [2*], Atsede G. Endegnanew[2], Magnus Korpås[3], Mattia Marinelli[1]

[1] Department of Electrical Engineering, Technical University of Denmark, 4000 Roskilde, Denmark
[2] Department of Energy Systems, SINTEF Energy Research, 7465 Trondheim, Norway
[3] Department of Electric Power Engineering, Norwegian University of Science and Technology, 7465 Trondheim, Norway
[*] salvatore.darco@sintef.no

Abstract: EV chargers can be controlled to support the grid frequency by implementing a standard-compliant fast Primary Frequency Control (PFC). This paper addresses potential effects on power systems due to control discreteness in aggregated electric vehicles (EVs) when providing frequency regulation. Possible consequences of a discrete response, as reserve provision error and induced grid frequency oscillations, are first identified by a theoretical analysis both for large power systems and for microgrids. Thus, an EV fleet management solution relying on shifting the droop characteristic for the individual EVs is proposed. The PFC is implemented in a microgrid with a Power-Hardware-in-the-Loop approach to complement the investigation with an experimental validation. Both the analytical and the experimental results demonstrate how the controller performance is influenced by the response granularity and that related oscillations can be prevented either by reducing the response granularity or by applying appropriate shifts on the droop characteristics for individual EVs.

1. Introduction

Frequency stability has been traditionally assured relying on ancillary services provided by conventional large power plants that are being partly replaced by renewable energy sources with an inherent stochastic behaviour. This may lead to the need of providing grid services relying more and more on small aggregated units connected to distribution grids. In this context, demand-side management is seen as a relevant prospective source of frequency regulation services such the Primary Frequency Control (PFC) [1]–[3].

Electric vehicles (EVs) are commonly considered flexible resources that can improve the energy management in power systems (e.g. smart-house nanogrids with solar generation [4]). However, several technical challenges may arise when EVs are aggregated and controlled to provide ancillary services. For example, the response time of single EVs as well as aggregated EV fleets is a critical aspect for enabling EVs participation in the reserve provision. Furthermore, the compliance of each EV charger with technical standards (e.g. IEC 61851 for AC charging [5] and IEC 15118 for DC charging possibly with vehicle-to-grid (V2G) [6]) along with the limitations in commercial standard-compliant hardware for EV charging [7], [8], require a given granularity when setting the charging rate.

This paper proposes an EV standard-compliant PFC whose performance is assessed under different power system conditions, by analysing the responsiveness of the regulating EVs when relying on discrete responses and when gradually reducing the charging rate granularity. Furthermore, an analysis of the possible consequences of the required granularity in the EV response is presented together with an EV fleet management solution to overcome such issues. The EV controller was tuned in a safe operating point and tested in a microgrid modelled to replicate the layout used in previous experimental research activities [9], [10]. Finally, laboratory results complement the granularity analysis with the employment of real hardware. The tests were carried out in a Power-Hardware-in-the-Loop (P-HiL) experimental environment [11], [12], where two 3-phase 60 kVA power converters connected to a 200 kVA grid emulator reproduced the behaviour of an EV fleet.

The definition of the PFC together with its theoretical analysis and experimental validation are original contributions to the existing literature as better clarified in Section 2 after a survey on the state-of-the-art for PFC provision from aggregated EVs. The proposed standard-compliant EV controller is described in Section 3 while Section 4 presents an analytical formulation to assess the effects of a discrete EV response and proposes an EV fleet management strategy. In Section 5 the P-HiL experimental validation is reported, and results are discussed. Conclusions are presented in Section 6.

2. EVs as PFC Providers: Literature Survey

The capability of EV fleets for provision of ancillary services for grid operators has been demonstrated in several technical and economic studies. Dynamic improvements in an islanded power system obtained with EV droop controllers are reported in [13]. [14], [15] demonstrate how large-scale utilization of EVs as a demand response resource can promote the development of wind power generation in Great Britain, also taking into consideration the EV users' travelling behaviour in the problem formulation. Similar results in [16]–[20] confirm the positive impact at a system level of EV charging control strategies in the presence of high penetration of generation from renewable energy sources. An economic

analysis of the value of these services for different countries is reported in [21]–[23].

The modelling of the aggregated response of an EV fleet and possible control strategy approaches are also investigated in many works. In [24] a discretised dispatch approach is utilized aiming to match the desired total power by means of an aggregator sending signals to turn EV chargers on or off according to a priority index. This control architecture is centralized and requires bidirectional real-time communication capabilities between the aggregator and the charging stations. In [25], [26] the communication requirements are drastically reduced by relying on a decentralized approach. In particular, in [26] the decision to change charging set-point is taken locally by the single EVs, while a remote centralized frequency measurement is performed by the aggregator and transmitted to each EV. Despite the potential positive effects, the aggregate response can cause power system issues when the share of EVs providing regulation is high and all the units respond to the same frequency signal. In this regard, accurate control strategies for EV fleets need to be implemented, which include proper overall response behaviour. Thus, [27] proposes a distributed frequency control that randomly assigns delays to each EV of the fleet. Additionally, [28] presents a novel methodology to design EV droop controllers and ensure the same stability margin with and without EVs participation to the PFC.

These literature references mostly focus on simulations, and experimental validation is rarely carried out. Moreover, an ideal EV power response is assumed and technical limitations due to standards requirements are neglected. Experimental testing has been performed in [29] to investigate the performance of a real charging EV at a charging post compliant with the IEC 61851. In [30] a charging algorithm based on a price signal is tested on commercial EVs, although without providing any ancillary services. By contrast, experimental activities validating how series-produced EVs can provide grid services have been carried out in [9] on an experimental testbed and in [31] on a real field test. These two references address also charging-related controllability limitations due to technical standards requirements and due to real commercially-available hardware, commonly neglected in most of the literature.

This paper investigates PFC implementation challenges in microgrids and in large power systems when accounting for the limitations due to components' design and technical standards requirements, and outlines a control strategy approach. Thus, the novelty of this paper compared to existing literature is threefold:

i) After developing a standard-compliant EV fast frequency controller, an analytical investigation on the consequences of a discrete EV response is presented, both in a large-size power system and in a microgrid;

ii) An EV fleet management solution to overcome related issues on an aggregated level is proposed;

iii) Results from a P-HiL experimental validation of the effectiveness of the EV controller are presented to complement the investigation.

3. Proposed Standard-Compliant EV Controller

This section presents the design and implementation of the proposed EV standard-compliant controller. Fast PFC is achieved by a joint action of all units providing grid services within the whole synchronous area when experiencing frequency deviations. This is normally achieved via droop controllers, meaning that governors operating in parallel share the load variation according to their rated power [32]. The droop constant K_{PFC_pow} in [W/Hz] represents the change in power output ΔP for a given frequency deviation Δf:

$$\Delta P = K_{PFC\_pow} \cdot \Delta f \tag{1}$$

In this study frequency regulation is provided via single-phase EVs by modulating their power consumption. As the technical standards IEC 61851 [5] and IEC 15118 [6] require the charging process to be regulated by setting the charging current, (1) can be rewritten as:

$$\Delta I_{PFC\_id} = K_{PFC} \cdot \Delta f \tag{2}$$

where ΔI_{PFC_id} is the ideal current variation that the EV would assure in case of a given Δf, and K_{PFC} is the *f-i* droop constant in [A/Hz].

In practice, the real current variation ΔI_{PFC} applied to the EV differs from ΔI_{PFC_id} mainly for three reasons. First, an upper limitation of the set-point is determined by the size of the breaker in the EV charger circuit (e.g. 16 A for the single-phase Mode2 charging). Second, EV technical standards impose constraints in the set-point granularity typically handled by aggregators and hardware manufactures with 1 A discreteness [7], [8]. Third, lower current limits are imposed by the standards for some charging modes (e.g. IEC 61851 requires a minimum current set-point of 6 A for Mode2 charging). Given these considerations, Fig. 1 shows the regulation curve in case of K_{PFC}=2.5 A/Hz (K_{PFC_pow}=575 W/Hz). The dashed line represents the ideal current variation ΔI_{PFC_id} while the solid one shows the real current variation ΔI_{PFC} with 1 A granularity.

Due to the required EV set-point limitations I_{lim} of 6 and 16 A, the EV's initial current set-point I_{init} is set at 11 A in order to have a symmetrical up/down regulation capability I_{reg} of ±5 A. This operating point corresponds to a stable system load condition at 50 Hz. The current reference I_{set} set by the controller on the EV charger is calculated as in (3), where the regulating contribution of the controller ΔI_{PFC} is positive or negative in case of over- or under-frequency, respectively.

$$I_{set} = I_{init} + \Delta I_{PFC} \tag{3}$$

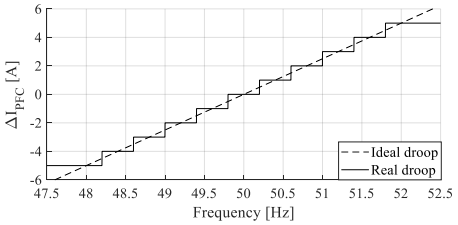

Fig. 1. *PFC ideal and discrete regulation curves.*

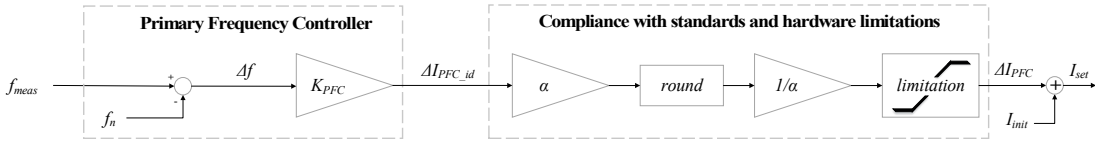

Fig. 2. *Block scheme for the implementation of the standard-compliant PFC.*

Fig. 2 depicts the block scheme of the EV control loop divided into two sub-groups. The first one concerns the implementation of Equation (2), to calculate the frequency deviation Δf and provides ΔI_{FPC_id} as output. This represents the input of the second group implementing the discrete characteristic and setting up/down current limitations. At each time step of the PFC operation, the output ΔI_{FPC} is then added to the central current set-point I_{init}, for which the system is considered stable at the nominal frequency. In order to implement a proper granularity in the EV response, the index α is introduced to indicate the amplitude of the steps when controlling the EV charging; $\alpha = \{1, 2, 4, \infty\}$ corresponds to the cases of granularity of 1 A, 0.5 A, 0.25 A and 0 A (which is the ideal continuous case), respectively. It is important to note that when controlling an EV charger the EV set-points represents the RMS values of the current waveform, and that in this study EVs are single-phase units charging in an uni-directional fashion according to charging Mode2.

It should be highlighted that the proposed controller can be implemented also for bi-directional V2G applications (i.e. when the battery power can flow in both directions). In this case, the initial current I_{init} is set to 0 A, and positive or negative current values will be set to charge or discharge the EV battery, respectively. Moreover, appropriate up/down limits will be set according to the type of charger. For example, limits of ±25 A were used for a ±10 kW rated charger in experimental tests on a IEC 15118-compliant V2G-capable hardware using the CHAdeMO protocol [33]. The characterization tests of such commercial hardware (operating in on-field projects) also confirmed the presence of similar 1 A current discreteness when setting the EV current set-point. Regarding the deployment of V2G technologies for the provision of grid services, one important consideration deserves to be mentioned also with regard to the additional wear of the EV battery during a PFC session. In particular, the V2G charging/discharging process may drastically impact the battery wear by even 0.4% of additional V2G-related cycle aging wear per year, considering daily 14 hours regulation sessions [22]. By contrast, uni-directional control of EVs does not have any negative effect on the battery lifetime, as the charging process is continuous during the PFC regulation process, yet at lower charging rates.

4. Effects of Granularity when Providing PFC

In this section, potential adverse effects generated by set-point granularity when aggregated EVs provide PFC are assessed. A generic power system with no specific configuration is assumed for the analysis. As first step, the case of an ideal EV response with no granularity when fixing the current set-point is proposed. A power equal to the contingency ΔP_{load} causing the imbalance is provided by conventional synchronous generators ΔP_{gen_id} and by the EVs ΔP_{EV_id} according to their droop coefficients as in (4) [34] in order to stabilize the frequency to a new steady-state value. For the sake of simplicity, the following formulation considers only one synchronous unit, whose governor droop is K_{gen}.

$$\begin{cases} \Delta P_{gen\_id} = \Delta P_{load} \cdot \frac{K_{gen}}{K_{PFC\_pow}+K_{gen}} \\ \Delta P_{EV\_id} = \Delta P_{load} \cdot \frac{K_{PFC\_pow}}{K_{PFC\_pow}+K_{gen}} = V_n \Delta I_{PFC\_id} \end{cases} \quad (4)$$

The ideal steady-state frequency value f_{eq_id} after the contingency is:

$$f_{eq\_id} = \frac{\Delta P_{load}}{K_{PFC\_pow}+K_{gen}} + f_n \quad (5)$$

Assuming nominal phase-to-neutral voltage conditions V_n, the EV contribution in terms of current ΔI_{PFC_id} is calculated using (2) and a linear droop while the corresponding power is ΔP_{EV_id}. In the realistic case of a given discreteness in the current set-point ($\alpha \neq \infty$), a step function as the solid curve in Fig. 1 is utilized. Thus, for a given measured frequency, the corresponding ideal current set-point is rounded up/down to the closest i-th value of the step function. The index i represents the i-th current set-point for a given granularity. The set current ΔI_{PFCi} is then calculated as:

$$\Delta I_{PFCi} = \alpha^{-1} \boldsymbol{round}(\alpha K_{PFC} \Delta f) \quad (6)$$

The current ΔI_{PFCi} will be set if the following condition is respected:

$$\Delta I_{PFC} = \Delta I_{PFCi}, if \ \Delta I_{PFC\_id} \in \{\Delta I_{PFCi\_min}; \Delta I_{PFCi\_max}\}$$

$$with \begin{cases} \Delta I_{PFCi\_min} = \Delta I_{PFCi} - 0.5\alpha^{-1} \\ \Delta I_{PFCi\_max} = \Delta I_{PFCi} + 0.5\alpha^{-1} \end{cases} \quad (7)$$

Such condition determines which set-point will be set on the EV, given the calculated ideal value and the implemented granularity α.

4.1. *Consequences in a Large Power System*

The main consequence related to the discreteness in the response for PFC is the inaccuracy in the primary reserve provision. This is identified as the difference ε_P between the requested (or expected) power to be exchanged with the grid P_{req} and the actual provided power P_{prov}:

$$\varepsilon_P = |P_{req} - P_{prov}| \quad (8)$$

The presence of such error difference in the reserve provision is due to the granularity of the set-points. In fact, the expected power is calculated with the ideal current set-point, derived by the linear ideal droop curve, whereas the actual delivered power is the result of the rounding. As the source of such error is the granularity in the current that is added to the initial

current set-point, (8) can be re-written in terms of current error as:

$$\varepsilon_I = \left| I_{req} - I_{prov} \right| \tag{9}$$

where I_{req} is the requested current calculated using the expected ideal change in the current ΔI_{PFC_id} in Equation (3) and I_{prov} is the actual current exchanged with the grid, obtained using ΔI_{PFC} in (3).

With reference to Equation (7), it can be noticed that for each *i*-th set-point the maximum error is given by the extreme values ΔI_{PFCi_max} and ΔI_{PFCi_min}. This means that the maximum error ε_{I_max} is defined as:

$$\varepsilon_{I\_max} = 0.5\alpha^{-1} \tag{10}$$

Higher granularity (i.e. smaller α) in the response leads to larger reserve provision errors when providing PFC. Fig. 3 reports a visual representation of the trend of the reserve provision error as a function of the requested current for a few granularity values. A granularity of 1 A (α = 1) implies a maximum error of 0.5 A, which represents 5% of the available regulating window I_{reg} of 10 A (i.e. the available reserve). For finer granularities the maximum error decreases proportionally: for α = 2 it is 0. 25 A (2.5% of I_{reg}), and for α = 4 it is 0. 125 A (1.25% of I_{reg}).

4.2. *Consequences in a Microgrid*

In low-inertia systems (e.g. in a microgrid), the discreteness in the response may cause effects related to the impossibility of reaching a stable steady-state frequency, f_{eq_id} in (5). This can lead to continuous oscillations between two consecutive current set-points. To better investigate such phenomena, the condition of setting a given set-point ΔI_{PFCi} reported in (7) can be re-written in terms of frequency limits, as in (11):

$$\Delta I_{PFC} = \Delta I_{PFCi}\,, \qquad if\ f_{meas} \in \{f_{i\_min};\ f_{i\_max}\}$$
$$with \begin{cases} f_{i\_min} = f_n - \frac{\Delta I_{PFCi\_min}}{K_{PFC}} \\ f_{i\_max} = f_n - \frac{\Delta I_{PFCi\_max}}{K_{PFC}} \end{cases} \tag{11}$$

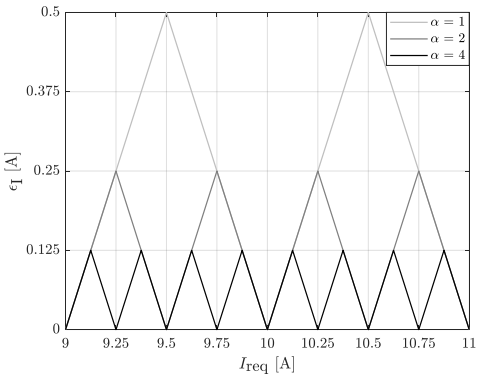

Fig. 3. *Response error as a function of the requested current for different granularities.*

Between two consecutive frequency intervals, a threshold value $f_{threshold(i;\, i-\alpha^{-1})}$ is defined equal to the minimum frequency value of the *i*-th step's interval f_{i_min} and the maximum value of the previous step $f_{(i-\alpha^{-1})\_max}$. In case of current oscillations, two different steady-state values calculated for the two consecutive current set-points would be below and above the threshold $f_{threshold(i;\, i-\alpha^{-1})}$, meaning that:

$$f_{i\_eq} < f_{threshold(i;\, i-\alpha^{-1})} < f_{(i-\alpha^{-1})\_eq} \tag{12}$$

where:

$$\begin{cases} f_{i\_eq} = f_n - \frac{\Delta P_{load} - V_n \Delta I_{PFCi}}{K_{gen}} \\ f_{threshold(i;\, i-\alpha^{-1})} = f_n - \frac{\Delta I_{PFCi} + 0.5\alpha^{-1}}{K_{PFC}} = f_n - \frac{V_n(\Delta I_{PFCi} + 0.5\alpha^{-1})}{K_{PFC\_pow}} \\ f_{(i-\alpha^{-1})\_eq} = f_n - \frac{\Delta P_{load} - V_n \Delta I_{PFC(i-\alpha^{-1})}}{K_{gen}} \end{cases} \tag{13}$$

The condition for current set-point oscillations between ΔI_{PFCi} and $\Delta I_{PFC(i-\alpha^{-1})}$ can be expressed as in (14):

$$f_{i\_eq} < f_{eq\_id} < f_{(i-\alpha^{-1})\_eq} \tag{14}$$

The condition in (14) is true whenever the steady-state frequency for any given current set-point differs from the ideal steady-state frequency value f_{eq_id} defined in (7). Thus, for any *i*-th set-point, the condition for two consecutive current set-point oscillations can be expressed as in (15) and in (16):

$$\forall\, i\,, f_{i\_eq} \neq f_{eq\_id} \tag{15}$$

which means:

$$V_n \alpha^{-1} \boldsymbol{round}(\alpha K_{PFC} \Delta f) \neq \Delta P_{load} \left(1 - \frac{K_{gen}}{K_{gen} + K_{PFC\_pow}}\right) \tag{16}$$

It can be noticed that the evaluation of these conditions depends on the tuning of the regulating units (K_{gen}, K_{PFC}, α), the magnitude of the contingency (ΔP_{load}), and on ΔI_{PFCi} that in turn depends on α, K_{PFC} and the measured frequency variation Δf. Unlike all the other parameters, the measured system frequency cannot be known a priori but can be estimated using Eq. (20) introduced in the next section. This includes parameters of the overall power system such as the total system inertia and the total apparent power of the rotating machines.

4.3. *A Smart Fleet Management Strategy*

A smart fleet management strategy is presented to tackle the two identified possible consequences of a discrete response. Even though the best solution would be to operate with a linear droop (i.e. ideal case with $\alpha = \infty$ associated to no provision error nor oscillations), this may not be achievable due to hardware and/or communication

limitations. However, an aggregated smoother response for the same granularity value can be still achieved if the EV fleet is properly managed. The proposed solution is based on the shift of the EV droop characteristics. For a given individual EV granularity $\alpha_{individual}$, it is possible to calculate an aggregated granularity α_{aggr} for a certain number of EVs n_{EV} as:

$$n_{EV} = \frac{\alpha_{aggr}}{\alpha_{individual}} \tag{17}$$

The shift of the discrete real droop f_{shift} is calculated as a translation along the x-axis in terms of frequency of the employed frequency-current droop curve and depends on the droop constant K_{PFC}. The shifts for each EV are calculated as:

$$f_{shift} = (2n_i + 1) \cdot (\pm \frac{0.5}{\alpha_{aggr} \cdot K_{PFC}}) \tag{18}$$

where:

$$n_i \in A, A = \{n \in N \mid n \leq (n_{EV}/2 - 1)\} \tag{19}$$

As an example, for the case of droop constant K_{PFC} = 2.5 A/Hz as in Fig. 1, from $\alpha_{individual}$ = 1 to α_{aggr} = 4 the number of needed EVs n_{EV} is four and the frequency shifts are ±0.05 and ±0.15 Hz. Fig. 4 shows the combination of the four shifted droop characteristics, along with the aggregated equivalent droop, which allows the EV aggregator to reduce the reserve provision error from 5% to 1.25%, which in terms of currents is from 0.5 to 0.125 A. For the sake of completeness, Tables 1-3 show the parameters for the implementation of the proposed smart fleet management strategy for the example cases of individual EV granularity of 1 A, 0.5 A and 0.25 A, respectively.

In general, the prevention of induced oscillations in a microgrid is not guaranteed since it is not certain that the ideal current value ΔI_{PFC_id} can be reached. However, this solution can drastically reduce the magnitude of such oscillations, which can then be damped more easily.

Table 1 Parameters in case of $\alpha_{individual}$ = 1

α_{aggr}	n_{EV}	n	f_{shift} [Hz]
2	2	0	±0.1
4	4	0; 1	±0.05; ±0.015
8	8	0; 1; 2; 3	±0.025; ±0.075; ±0.0125; ±0.175
16	16	0; 1; 2; 3; 4; 5; 6; 7	±0.0125; ±0.0375; ±0.0625; ±0.0875; ±0.1125; ±0.1375; ±0.1625; ±0.1875

Table 2 Parameters in case of $\alpha_{individual}$ = 2

α_{aggr}	n_{EV}	n	f_{shift} [Hz]
4	2	0	±0.05
8	4	0; 1	±0.025; ±0.075
16	8	0; 1; 2; 3	±0.0125; ±0.0375; ±0.0625; ±0.0875

Table 3 Parameters in case of $\alpha_{individual}$ = 4

α_{aggr}	n_{EV}	n	f_{shift} [Hz]
8	2	0	±0.025
16	4	0; 1	±0.0125; ±0.0375

5. Assessment of EV Response Granularity in a P-HiL Experimental Environment

The main purpose of the proposed experimental investigation is to sensitively assess the consequences on the system dynamics of a set of EVs performing simultaneous regulation with discrete responses. Different levels of granularity when setting the EV charging current are considered and results are compared with the ones expected from the analysis in Section 4. In this section, the experimental test-bed is presented along with its implementation within a P-HiL laboratory test environment. Then, the tested scenarios are defined and relevant results are presented and discussed.

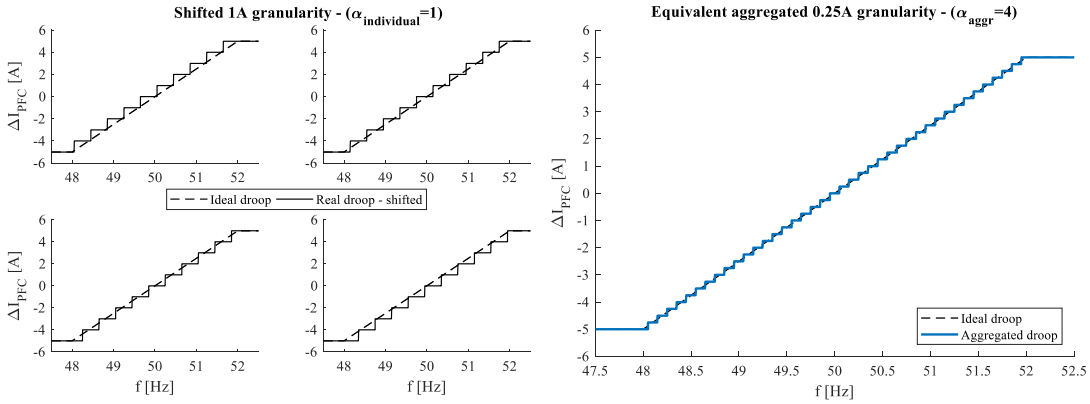

Fig. 4. PFC ideal and discrete regulation curves of the single EVs and of the aggregated equivalent fleet.

5.1. *Microgrid Layout and P-HiL Experimental Setup*

The tested microgrid aims at representing one islanded configuration for the experimental LV flexible grid SYSLAB previously utilized in [9]. The only unit that provides rotating inertia to the system is a diesel-set synchronous generator with two pole pairs p, rated apparent power S_{gen} = 60 kVA (nominal active power P_{gen} = 48 kW), and inertia constant $2H$ = 2 s. Thus, a change in the difference between mechanical power P_m and electrical power P_e would be reflected in a change in the system frequency as described by (20) [34]:

$$P_m - P_e = \frac{2H \cdot S_{gen} \cdot \frac{d\omega}{dt}}{\omega_n} \quad (20)$$

where ω is the angular velocity of the rotor [rad/s] and ω_n is its nominal value, obtained as:

$$\omega_n = \frac{2\pi \cdot f_n}{p} \quad (21)$$

The governor of the diesel turbine operates with a droop K_{gen} of 2 kW/Hz. A static load P_{load} of 15 kW is constantly connected to the generator and is increased/decreased to obtain frequency dynamics according to (21) that will be enhanced by the implemented EV controllers. A few EVs are connected to the same busbar, with the option of activating the proposed PFC controller in case of contingency. A schematic representation of the described microgrid is shown in Fig. 5.

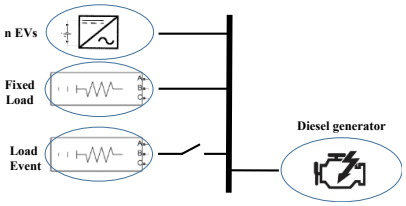

Fig. 5. *Microgrid layout.*

P-HiL experiments have been carried out at the Norwegian National Smart Grid Laboratory (NSGL), located in Trondheim at the campus of the Norwegian University of Science and Technology (NTNU) and jointly operated by SINTEF and NTNU [35]. The P-HiL hardware equipment utilized for the tests consists of a 200 kVA, 5 kHz bandwidth power amplifier from Egston Power, the real time simulator OPAL-RT OP5600 unit OP4520 extension box and two 60 kW two-level three-phase converters. Either one or two of the converters (depending on the tested scenario) are assumed as the *hardware under test (HuT)*. The converters can reproduce the aggregated behaviour of up to twelve single-phase EVs charging simultaneously according to Mode2 operation mode. The EV batteries are connected to the DC link, whose voltage is kept constant at 680 V by a third converter (identical to the ones described above) that is constantly operating as constant DC voltage source. The P-HiL experimental setup is depicted in Fig. 6, where the three main parts of the typical P-HiL setup are highlighted, namely the *digital simulation system*, the interface with *power amplifier*, and the *HuT* [11], [36], [37].

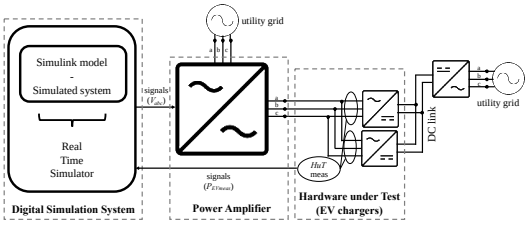

Fig. 6. *P-HiL experimental setup.*

The available *digital simulation system* has an Intel processor with 12 cores and a clock of 3.46 GHz. However, only 3 cores have been utilized for the presented experiments: one for the controller of the converters, one for the power amplifier, and one for the modelling of the power system. As for the generation of the voltage signals that the *power amplifier* sets at its output channels, the block diagram in Fig. 7 has been implemented in the *digital simulation system* utilizing Simulink in Matlab 2013a with simulation time step equal to 0.2 ms. It needs an RMS phase-to-neutral voltage reference value V_{ref} manually set equal to 230 V, and it considers the active power measurements at the AC side of the two converters under study, namely P_{EVmeas} in Fig. 7. Considering a given electrical load (with eventual steps) and the emulated power system parameters listed in the previous subsection, the implementation of (20) enables the calculation of the rate of change of the angular velocity $d\omega/dt$. This value can be integrated twice to obtain the reference angle θ for the generation of the microgrid AC voltages.

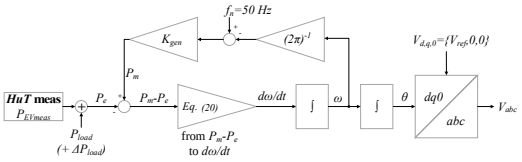

Fig. 7. *Generation of the three-phase voltage reference signals as output of the power amplifier.*

The EV current set-points to be set on the physical converters are computed as described in Section 3. With reference to the block diagram in Fig. 2, it should be noted that multiple EV set-points can be computed independently in order to emulate the case of more EVs with different time responsiveness, droop coefficients or granularities. In fact, before aggregating them, each EV can receive the same or a different set-point, for instance, according to eventual droop shifts in case of the implementation of the proposed droop shift-based fleet management logic.

5.2. *Definition of Scenarios*

The investigation is carried out by monitoring the system frequency dynamics after a contingency. Each study case is tested with a given load step taking place on a stable operating condition with f = 50 Hz. With reference to the microgrid layout presented in Fig. 5, the resistive load is set to 15 kW, while three single-phase EVs are considered within the fleet, each one charging with RMS current I_{init} = 11 A which corresponds to an aggregated EV fleet power P_{init} of

7.59 kW. Therefore, the total load that the emulated synchronous generator supplies at the initial equilibrium condition amounts to 22.59 kW, which corresponds to a loading factor of almost 50%, being the active power generation capability of the gen-set unit P_{gen} is 48 kW. The grid contingency is obtained with a load increment ΔP_{load} of 2 kW, which causes under-frequency conditions.

The EV controller parameters are set considering a safe operating condition, as the one utilized in previous experimental activities [9], [10]. In particular, the implemented K_{PFC} droop coefficient of 2.5 A/Hz means a total power droop for 3 EVs of 1.725 kW/Hz, which is very close to the droop implemented in the diesel generator set (2 kW/Hz). This enables the investigation of a realistic scenario with EVs reacting with similar response sensitiveness as conventional generating units. The parameters of the implemented PFC are reported in Table 4.

Table 4 Implemented PFC parameters

PFC parameter	Values set for the experimental validation
I_{reg}	10 A (±5 A)
I_{lim}	6-16 A
I_{init}	11 A
K_{PFC}	2.5 A/Hz
K_{PFC_pow}	575 W/Hz
K_{PFC_pow} *(for 3 EVs)*	1725 W/Hz
α	$\{1, 2, 4, \infty\}$ $\{1, 0.5, 0.25, 0\}$A

The initial absorbed power P_{init} ($=3I_{init}V_n$=7.59 kW) corresponds to 15.8% of the microgrid generation capacity P_{gen}. This percentage can appear as a very high share, but is roughly the same order of magnitude as a forecasted future scenario in the Nordic synchronous area. In fact, from the *Nordic EV Outlook 2018* report [38], the number of EVs in the Nordics is forecasted to be of 4 million, whereas the Nordic generation capacity is 103 GW, as stated in the *Nordic Market Report* [39]. In the worst-case scenario where all EVs charge simultaneously, the corresponding initial absorbed power amounts to about 10 GW, which represents a share of about 10% of the installed Nordic generation capacity.

The implemented diesel gen-set droop K_{gen} (=2 kW/Hz) corresponds to 48% droop on system base. This represents a high value when compared to hydro and gas power plants. However, if seen from a system point of view, it can represent a realistic case given the increasing penetration of uncontrolled small wind and solar plants that contribute to increase the total generation capacity without increasing the system absolute droop K_{gen}. High values mean that the conventional generator reacts smoothly, leaving space for regulation to other non-conventional units, such as EV fleets. These conditions may appear in islanded power systems or microgrids, where frequency regulation from small distributed energy resources will be crucial when increasing the penetration of renewables.

5.3. Results of Experimental Assessment

As first step, the same islanded configuration tested in previous experimental activities [9] and presented in subsection 5.1 is re-proposed. In this case a granularity of 1 A was implemented (α = 1). Fig. 8 shows results from the uncontrolled EV case and the case of PFC provision in an experimental microgrid with real EVs. Due to the discrete EV response, in case of PFC the current absorbed by one EV oscillates between two consecutive set-points, as none of them can allow a steady-state frequency to be reached without passing the threshold that triggers the consecutive set-point. This aspect is of outmost importance and therefore is tackled herein below by means of P-HiL experiments.

The first P-HiL test results are reported in Fig. 9, which shows the uncontrolled EV case. P-HiL tests match the ones reported in Fig. 8, with an after-contingency steady-state frequency of 49 Hz. This value is motivated by the fact that the PFC actions are deactivated, and after the 2 kW contingency, frequency regulation is provided only by the diesel gen-set, whose governor acts with a droop K_{gen} of 2 kW/Hz.

To complement the analytical formulation proposed in Section 4, Fig. 10 reports results from experimental P-HiL tests with PFC implemented as described in Section 3 for four different granularity cases: α = {1, 2, 4, ∞}, corresponding to the cases of granularity of 1 A, 0.5 A, 0.25 A and 0 A, respectively. Firstly, it can be observed that the controller is tuned in a safe operation zone since system instabilities do not occur. Secondly, it can be noticed that the 1-A oscillations found in the previous experimental work in Fig. 8 are

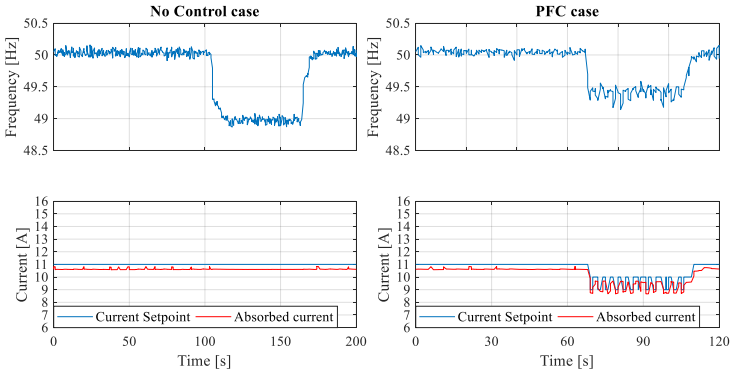

Fig. 8. *Experimental results with 3 EVs obtained in previous experimental works [9]. A granularity of 1 A is implemented (α=1).*

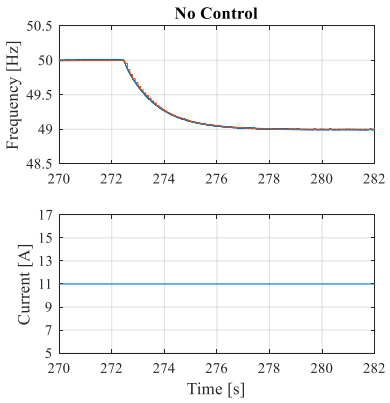

Fig. 9. *P-HiL experimental results: Frequency and EV current set-points for the uncontrolled EV case.*

replicated. Thanks to the flexibility of the P-HiL test setup, a deeper and more exhaustive investigation is possible. In particular, the cases of finer granularities are studied, and the experimental results are evaluated against the analytical formulations described in Section 4. From Fig. 10, it can be seen that oscillations take place even for the 0.5 A and 0.25 A discreteness cases, as none of the considered granularities leads to the ideal steady-state frequency value f_{eq_id} which is 49.463 Hz. Such value of f_{eq_id} is calculated using Equation (8) and confirmed from the P-HiL results when $\alpha = \infty$. For the three discrete response cases, current set-point oscillations appear because the condition in (14) is matched, and the threshold $f_{threshold(i;\, i-\alpha^{-1})}$ between two consecutive set-points is crossed. However, the case $\alpha = 4$ shows very limited frequency oscillations, that can be achieved either via such a very fine granularity or by smartly controlling the individual EV set-point as proposed smart EV fleet strategy. An analogue response could have been obtained if four EVs are controlled with shifted 1-A step functions. This is the case of applying horizontal shifts to the f-i step droop functions by f_{shift} of ±0.05 and ±0.15 Hz, obtaining $\alpha_{aggr} = 4$ (0.25 A granularity) relying on implementation of 1-A step functions for each individual EV ($\alpha_{individual} = 1$).

Table 5 reports steady-state frequency values for the consecutive set-points where the oscillations take place for different granularity cases, which confirm that the above-presented oscillation conditions are respected. In fact, the numerical results calculated as explained in Section 4 match the P-HiL experimental results reported in Fig. 10. For $\alpha = 1$ the current set-point oscillates between 10 and 9 A, for $\alpha = 2$ between 10 and 9.5 A, and for $\alpha = 4$ between 9.75 and 9.5 A.

Table 5 Results from experimental PFC activities

	$\alpha = 1$	$\alpha = 2$	$\alpha = 4$
ΔI_{PFCi}	-1 A	-1 A	-1.25 A
$\Delta I_{PFC(i-\alpha^{-1})}$	-2 A	-1.5 A	-1.5 A
f_{i_eq}	49.345 Hz	49.345 Hz	49.431 Hz
$f_{(i-\alpha^{-1})\_eq}$	49.690 Hz	49.518 Hz	49.518 Hz
$f_{threshold(i;\, i-\alpha^{-1})}$	49.400 Hz	49.500 Hz	49.450 Hz
f_{eq_id} ($\alpha = \infty$)	49.463 Hz	49.463 Hz	49.463 Hz
$\Delta I_{PFC\ id}$ ($\alpha = \infty$)	-1.3425 A	-1.3425 A	-1.3425 A

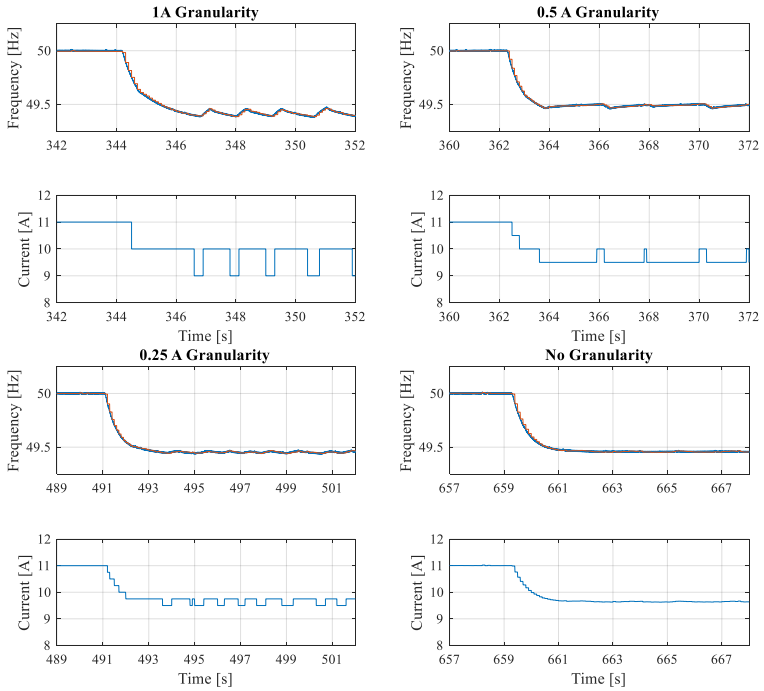

Fig. 10. *P-HiL experimental results: Frequency and current set-points for the EV response granularity sensitivity analysis.*

6. Conclusions

This work investigated the impact of discrete responses of aggregated EVs providing primary frequency regulation. An droop-based primary frequency controller was implemented considering EV standards and commercial hardware limitations. The crucial role played by the EV current set-point granularity was analytically investigated assessing the consequences in applications in microgrids and large-scale power systems, and a smart EV fleet management strategy to overcome related issues was proposed. The analysis was complemented with real time P-HiL experimental tests in a microgrid. The microgrid was modelled within the P-HiL setup, and the PFC for EVs was tuned to operate in a safe operating zone.

Results from the experimental tests show the expected frequency oscillations due to the controller's discrete nature when setting the current set-points. Frequency oscillations are experimentally decreased by gradually reducing the amplitude of the required EV charging rate granularity, and the experimental results matched the numerical results obtained via the analytical formulation proposed in the paper. To prevent any possible frequency oscillations, the authors recognize that a continuous regulation may be necessary for microgrid applications, but this is not easily achievable due to standards and hardware limitations. Nevertheless, with the proposed EV fleet management method it is possible to achieve an aggregated response with an equivalent granularity lower than the one implemented on each individual EV. Although the major consequence of EV discrete regulation in large-scale power system was identified as primary reserve provision mismatches, oscillations phenomena may take place in case a considerable number of EVs respond simultaneously to the same discrete charging/discharging signal. Thus, a smooth overall response may be needed to prevent system issues also on large-scale applications. This can be achieved either by making the regulation continuous, or by introducing additional requirements on the whole aggregated EV fleet response, for instance by means of overall ramping rate or fleet time response. Another interesting subject for further investigations is to perform a more detailed analysis of the aggregated frequency response on a system level. It was shown that it is possible to mitigate some of the effects of response discretization by shifting the droop response of individual EVs. In areas with hundreds of thousands of EVs, such as the Nordic system, a smoother aggregated response could for example be achieved by using probability functions for the individual droop shifting functions. Further power system studies are needed to e.g. analyse how much thermal power generation reserves that can actually be displaced using different aggregation strategies for EVs, when considering different scenarios for the future generation mix, demand and grid development. These aspects are being investigated within future works.

7. Acknowledgments

The work in this paper was supported by the European Commission, under the FP7 project ELECTRA (Grant No.: 609687). More information at www.electrairp.eu

8. References

[1] D. S. Callaway and I. A. Hiskens, "Achieving Controllability of Electric Loads," *Proc. IEEE*, vol. 99, no. 1, pp. 184–199, Jan. 2011.

[2] E. Vrettos, C. Ziras, and G. Andersson, "Fast and Reliable Primary Frequency Reserves from Refrigerators with Decentralized Stochastic Control," *IEEE Trans. Power Syst.*, vol. 32, no. 4, pp. 2924–2941, 2017.

[3] C. Gouveia, C. L. Moreira, J. Abel, P. Lopes, and D. Varajão, "Microgrid Service Restoration," *IEEE Ind. Electron. Mag.*, vol. 7, no. 4, pp. 26–41, 2013.

[4] X. Wu, X. Hu, Y. Teng, S. Qian, and R. Cheng, "Optimal integration of a hybrid solar-battery power source into smart home nanogrid with plug-in electric vehicle," *J. Power Sources*, vol. 363, pp. 277–283, 2017.

[5] IEC 61851-1:2010, "Electric vehicle conductive charging system – Part 1: General requirements." 2010.

[6] IEC/ISO 15118-1:2013, "Road vehicles — Vehicle to grid communication interface — Part 1: General information and use-case definition." 2013.

[7] "Nissan, enel and nuvve operate world's first fully commercial vehicle-to-grid hub in denmark," 2016. [Online]. Available: http://www.nissan-helsingor.dk/index.php/om-os/nyheder/show/news/id/4. [Accessed: 19-Oct-2018].

[8] Phoenix Contact, "EV Charge Control: Standard-compliant control of the Control Pilot and Proximity Plug interfaces between the electric vehicle and charging station. (User manual)." 2015.

[9] M. Rezkalla, A. Zecchino, S. Martinenas, A. M. Prostejovsky, and M. Marinelli, "Comparison between synthetic inertia and fast frequency containment control based on single phase EVs in a microgrid," *Appl. Energy*, 2017.

[10] M. Marinelli, S. Martinenas, K. Knezović, and P. B. Andersen, "Validating a centralized approach to primary frequency control with series-produced electric vehicles," *J. Energy Storage*, vol. 7, pp. 63–73, 2016.

[11] E. De Jong *et al.*, "European White Book on Real-Time Powerhardware-in-the-Loop testing," Arnhem, Netherlands, 2011.

[12] O. Mo, S. D' Arco, and J. A. Suul, "Evaluation of Virtual Synchronous Machines With Dynamic or Quasi-Stationary Machine Models," *IEEE Trans. Ind. Electron.*, vol. 64, no. 7, pp. 5952–5962, 2017.

[13] P. M. R. Almeida, F. J. Soares, and J. A. P. Lopes, "Electric vehicles contribution for frequency control with inertial emulation," *Electr. Power Syst. Res.*, vol. 127, pp. 141–150, 2015.

[14] Y. Mu, J. Wu, J. Ekanayake, N. Jenkins, and H. Jia, "Primary frequency response from electric vehicles in the Great Britain Power System," *IEEE Trans. Smart Grid*, vol. 4, no. 2, pp. 1142–1150, 2013.

[15] J. Meng, Y. Mu, H. Jia, J. Wu, X. Yu, and B. Qu, "Dynamic frequency response from electric vehicles considering travelling behavior in the Great Britain power system," *Appl. Energy*, vol. 162, pp. 966–979, 2016.

[16] X. Luo, S. Xia, and K. W. Chan, "A decentralized charging control strategy for plug-in electric vehicles to mitigate wind farm intermittency and enhance frequency regulation," *J. Power Sources*, vol. 248, pp. 604–614, Feb. 2014.

[17] S. Izadkhast, P. Garcia-Gonzalez, and P. Frías, "An Aggregate Model of Plug-In Electric Vehicles for Primary Frequency Control," *IEEE Trans. Power Syst.*, vol. 30, no. 3, pp. 1475–1482, 2015.

[18] H. Liu, Z. Hu, Y. Song, and J. Lin, "Decentralized Vehicle-to-Grid Control for Primary Frequency Regulation Considering Charging Demands," *IEEE Trans. Power Syst.*, vol. 28, no. 3, pp. 3480–3489, Aug. 2013.

[19] H. N. T. Nguyen, C. Zhang, and J. Zhang, "Dynamic Demand Control of Electric Vehicles to Support Power Grid With High

Penetration Level of Renewable Energy," *IEEE Trans. Transp. Electrif.*, vol. 2, no. 1, pp. 66–75, 2016.
[20] H. Liu, Z. Hu, Y. Song, J. Wang, and X. Xie, "Vehicle-to-Grid Control for Supplementary Frequency Regulation Considering Charging Demands," *IEEE Trans. Power Syst.*, vol. 30, no. 6, pp. 3110–3119, 2015.
[21] P. Codani, M. Petit, and Y. Perez, "Participation of an electric vehicle fleet to primary frequency control in France," *Int. J. Electr. Hybrid Veh.*, vol. 7, no. 3, p. 233, 2015.
[22] A. Thingvad, C. Ziras, and M. Marinelli, "Economic value of electric vehicle reserve provision in the Nordic countries under driving requirements and charger losses," *J. Energy Storage*, vol. 21, no. November 2018, pp. 826–834, 2019.
[23] S. Han and S. Han, "Economic feasibility of V2G frequency regulation in consideration of battery wear," *Energies*, vol. 6, no. 2, pp. 748–765, 2013.
[24] E. Sortomme and K. W. Cheung, "Intelligent Dispatch of Electric Vehicles Performing Vehicle-to-Grid Regulation," in *2012 IEEE International Electric Vehicle Conference*, 2012, pp. 1–6.
[25] A. Molina-garcía, F. Bouffard, and D. S. Kirschen, "Decentralized Demand-Side Contribution to Primary Frequency Control," *IEEE Trans. Power Syst.*, vol. 26, no. 1, pp. 411–419, 2011.
[26] M. González Vayá and G. Andersson, "Combined Smart-Charging and Frequency Regulation for Fleets of Plug-in Electric Vehicles," in *2013 IEEE Power & Energy Society General Meeting*, 2013, pp. 1–5.
[27] M. R. V. Moghadam, R. Zhang, and R. T. B. Ma, "Distributed Frequency Control via Randomized Response of Electric Vehicles in Power Grid," *IEEE Trans. Sustain. Energy*, vol. 7, no. 1, pp. 312–324, 2016.
[28] S. Izadkhast, P. Garcia-Gonzalez, P. Frìas, L. Ramìrez-Elizondo, and P. Bauer, "An Aggregate Model of Plug-in Electric Vehicles Including Distribution Network Characteristics for Primary Frequency Control," *IEEE Trans. Power Syst.*, vol. 31, no. 4, pp. 2987–2998, 2016.
[29] F. Lehfuss, M. Nöhrer, M. Faschang, S. Ledinger, and F. Kupzog, "Comprehensive Infrastrusture for Electric Vehicle Charging Interoperability and Grid Compliance Testing," *Int. J. Distrib. Energy Resour. Smart Grids*, pp. 29–42, 2015.
[30] R. Abousleiman and R. Scholer, "Smart charging: System design and implementation for interaction between plug-in electric vehicles and the power grid," *IEEE Trans. Transp. Electrif.*, vol. 1, no. 1, pp. 18–25, 2015.
[31] K. Knezović, S. Martinenas, P. B. Andersen, A. Zecchino, and M. Marinelli, "Enhancing the Role of Electric Vehicles in the Power Grid : Field Validation of Multiple Ancillary Services," *IEEE Trans. Transp. Electrif.*, vol. 3, no. 1, pp. 201–209, 2016.
[32] ENTSO-E, "Frequency Stability Evaluation Criteria for the Synchronous Zone of Continental Europe - Requirements and impacting factors," Brussels, Belgium, 2016.
[33] A. Zecchino, A. Thingvad, P. B. Andersen, and M. Marinelli, "Suitability of Commercial V2G CHAdeMO Chargers for Grid Services," in *EVS 31 & EVTeC 2018*, 2018, pp. 1–7.
[34] P. Kundur, *Power system stability and control*. 1994.
[35] "National Smart Grid Laboratory." [Online]. Available: https://www.sintef.no/en/all-laboratories/smartgridlaboratory/. [Accessed: 31-Jul-2017].
[36] C. Seitl, J. Kathan, G. Lauss, and F. Lehfuss, "Power hardware-in-The-loop implementation and verification of a real time capable battery model," in *IEEE International Symposium on Industrial Electronics*, 2014, pp. 2285–2290.
[37] Q. Hong, I. Abdulhadi, A. Roscoe, and C. Booth, "Application of a MW-Scale Motor-Generator Set to Establish Power-Hardware-in-the-Loop Capability," in *presented at IEEE International Conference on Innovative Smart Grid Technologies IEEE ISGT Europe 2017*, 2017, pp. 1–6.
[38] IEA International Energy Agency, "Nordic EV Outlook 2018," 2018.
[39] Nordic Energy Regulators NordREG, "Nordic Market Report," 2014.